High-energy $(e,2e)$ spectrometer for the study of the spectral momentum density of materials

M. Vos, G. P. Cornish, and E. Weigold
Atomic and Molecular Physics Laboratory, Research School of Physical Sciences and Engineering, The Australian National University, Canberra ACT 0200, Australia

(Received 16 May 2000; accepted for publication 10 July 2000)

A new spectrometer for the study of energy-resolved momentum densities is described. The $(e, 2e)$ spectrometer uses a symmetric configuration and uses incoming energies up to 50 keV. Energy resolution and momentum resolution are 1.8 eV and 0.1 a.u., respectively. Compared to previous spectrometers this spectrometer has rather low levels of multiple scattering, and thus allows for more quantitative analysis of the data and/or the measurement of thicker samples. © *2000 American Institute of Physics.* [S0034-6748(00)04310-0]

I. INTRODUCTION

In an electron momentum spectroscopy (EMS) experiment an incoming electron ionizes the target and the scattered and ejected electron are detected in coincidence.[1–3] If both the scattered and ejected particle have a high enough energy the ionizing collision can be described using the plane-wave impulse approximation and, within a one particle approximation, one can, using the laws of energy and momentum conservation, infer the binding energy and the momentum of the ejected electron before the collision. The measured intensity distribution of coincident events is then simply proportional to the probability that a target electron has a certain binding energy-momentum combination.

For a system of interacting electrons the naive image sketched above has to be modified slightly. The $(e, 2e)$ event itself remains a collision between two electrons only. The measured intensity, however, cannot be compared to simple orbitals but is now proportional to the spectral function of the interacting electron gas. Recently, it has become possible to calculate spectral functions of *real* solids and the results tend to deviate strongly from the effective one-particle theories (e.g., band structure calculations), with large differences also occurring between the different many-body theories.[4] EMS seems to be the ideal vehicle to test these theories. Indeed for gas-phase experiments EMS has already a strong track record in elucidating correlation effects.[1,3]

For solids the technique should work just as well as for gaseous targets, provided that multiple scattering in the incoming and two outgoing electron beams can be reduced to a manageable level. The main multiple scattering events are inelastic collisions, such as plasmon creation, and (elastic) deflections from nuclei. Although these multiple scattering events are reasonably well understood, and their magnitude can be estimated,[5] they obscure, if occurring too frequently, direct comparison with theory. These experiments are done in a transmission geometry and as there is a limit to how thin one can make a film, the only way to further reduce the multiple scattering is increasing the energy of the incoming and outgoing electrons, resulting in an increase of the mean free path for both elastic and inelastic scattering. However, with the increase of the transferred momentum in the binary electron–electron collision the Mott cross section for electron–electron scattering decreases strongly. Thus the challenge is to increase the transferred momentum without sacrificing the coincidence count rate. This is the design goal of the spectrometer described in this article.

II. DEVELOPMENT OF EMS OF SOLIDS

The first EMS experiment on solids was done about 30 years ago, and clearly showed that the carbon core level had a momentum distribution that differed from the valence band.[6] Improvement in energy resolution allowed Ritter and co-workers to resolve structure within the valence band.[7] These experiments were hampered by rather unpractical low coincidence count rates and poor energy and momentum resolution. In order to resolve the count rate problem it was necessary to develop multidimensional electron detection techniques, allowing for the simultaneous measurement of a series of energies[8,9] and later the simultaneous measurement of a range of both energies and angles (i.e., momenta) at Flinders University.[10]

The last spectrometer was very successful in measuring a range of specimens, showing clearly the dispersion of binding energy with momentum of the quasiparticle peaks. However, it became clear that multiple scattering was severely affecting quantitative interpretation of the measured intensities. In spite of this, it was evident that for an understanding of the measured intensities one must go beyond band structure calculations that take into account electron–electron correlation in an average way.[11]

In recent years there has been some success in studying the $(e, 2e)$ reaction with solids in a reflection geometry at relatively low energies.[12,13] These experiments have the great advantage that they do not require thin samples. The interpretation is however much more difficult as, at these energies, the cross section cannot be described as a product of a factor related to the target electronic structure and a factor determined by only the electron–electron collision. The reaction mechanism is very complicated with the continuum electron waves being far from plane waves. These experi-

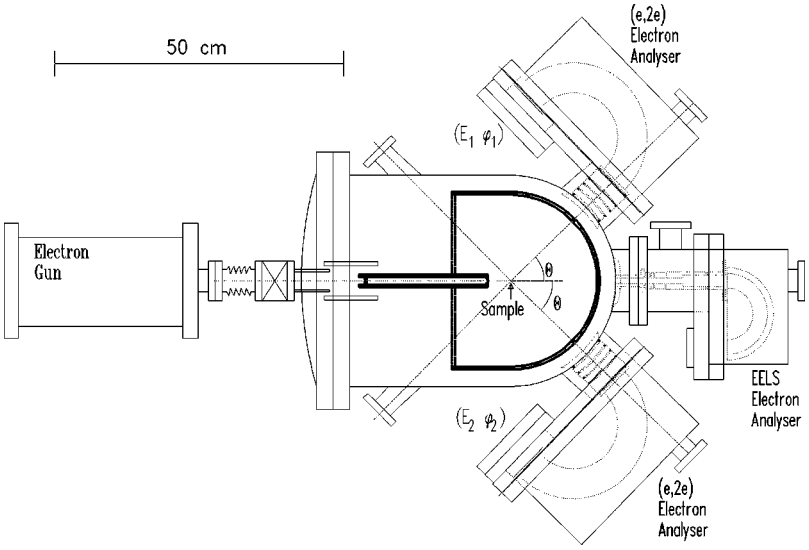

FIG. 1. Outline of the new spectrometer. The positive high voltage area is indicated by the thick line. The electron optics is shown as dotted lines.

ments are as a consequence very interesting for the study of electron–electron collisions in solids, but as the information obtained does not describe the target spectral function directly, it seems that at present the information obtained by reflection-type $(e, 2e)$ experiments must be considered as complimentary to that obtained from high-energy transmission EMS experiments, rather than the equivalent.

Another class of $(e, 2e)$ experiments, at energies much higher than those described here, are the inner shell excitation studies on heavy elements as done by Nakel and co-workers.[14]

III. DESIGN CRITERIA

The design has to be a compromise between two opposing tendencies. Higher incoming and outgoing energies means larger mean free path, so that for a given specimen thickness (of the order of 10 nm) a smaller fraction of the electrons will suffer multiple scattering. Thus, for aluminum the inelastic and elastic mean free paths at 20 keV are $\simeq$23 nm and $\simeq$19 nm, respectively, whereas at 1 keV they are 2 and 1 nm, respectively. However, higher energies also means a larger transferred momentum and hence a smaller cross section of the $(e, 2e)$ reaction. In principle the decrease in cross section can be compensated by an increase in beam current. In practice beam current greater than about 10 μA are impractical as damage to the sample and space charge induced energy broadening become significant. Higher energies also increase the demand on the power supplies, as the required energy resolution of the order of 1 eV requires a stability of the power supplies of a few tenths of 1 eV over the measurement period (typically a few days).

These considerations lead to a design of a spectrometer using a 50 keV incoming beam (E_0) and a symmetric scattering geometry, with both outgoing electrons at a nominal energy (E_1 and E_2) of 25 keV. In comparison with the asymmetric Flinders spectrometer, which uses an incident energy of 20 keV and outgoing energies of 18.8 and 1.2 keV, the lowest energy of any electron involved has increased from 1.2 to 25 keV, and hence multiple scattering effects should decrease by a factor of 20. As a consequence the cross section has also decreased by about two orders of magnitude.

IV. SPECTROMETER GEOMETRY

A schematic layout of the spectrometer is shown in Fig. 1. An electron gun (based on the design of Schmoranzer *et al.*,[15] using a LaB_6 filament) produces a 25 keV electron beam relative to ground. The target is in a large hemisphere which is at +25 kV. Thus inside this sphere the incoming electrons have a kinetic energy E_0 of 50 keV. Here the incoming beam is well collimated by two apertures, one 0.2 mm in diameter, just inside the high voltage area, and one 0.1 mm in diameter near the sample. The apertures are 20 cm apart, so the momentum of the incoming electrons is accurately determined.

The sample is positioned in the center of the high voltage hemisphere. Two narrow slits are positioned symmetrically in the high voltage hemisphere at polar angles of 44.3°. Due to relativistic corrections the Bethe ridge condition (describing the scattering of an electron by a stationary free electron) corresponds to polar angles slightly less than 45° for a symmetric scattering geometry and are somewhat dependent on E_0. The emerging electrons leave the sample with energy E_1 and E_2 (both close to $0.5E_0$) and are decelerated on leaving the high voltage hemisphere and subsequently analyzed for energy and azimuthal angle.

This high-voltage layout is quite similar to that used by Ritter.[7] In our case there are three reasons for adopting this high voltage design. In the first place we have to handle only voltages of a magnitude of 25 kV. This is much easier than handling voltages of 50 kV in vacuum. In the second place the electron detectors are close to ground, which facilitates the coupling out of the detector signal to the electronics. Finally this approach helps us meet the power supply stability requirement. This is explained in Fig. 2. The potential of the filament in the electron gun is $V^-_{\text{main}}+V_{\text{gun offset}}$. The potential of the target is V^+_{main}. The mean voltage of both analyzers is V_{analyzer}. Assume that in detector 1 we detect an electron with pass energy E_1^{PE} and in analyzer 2 an electron

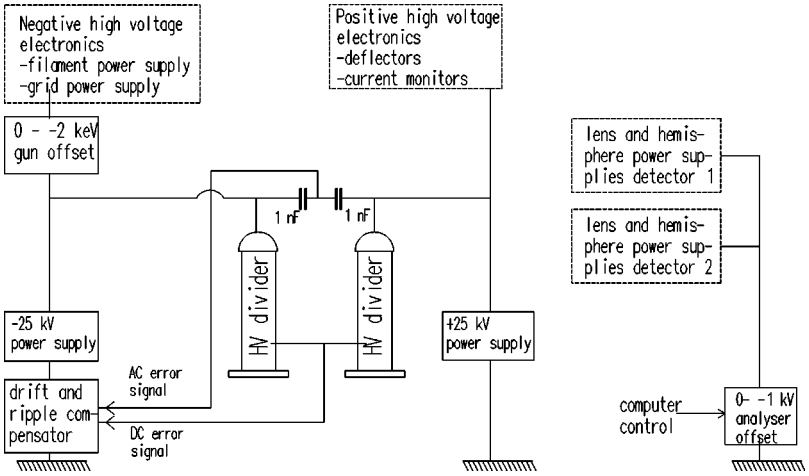

FIG. 2. Overview of the high voltage electronics used in the spectrometer and its stabilization system.

with energy E_2^{PE}. If these are the scattered and ejected electron from the same ionizing event the corresponding binding energy ε in eV is given by

$$\varepsilon = E_0 - E_1 - E_2 = q(V_{\mathrm{main}}^- + V_{\mathrm{gun\ offset}} + V_{\mathrm{main}}^+ - 2V_{\mathrm{analyzer}}) - E_1^{\mathrm{PE}} - E_2^{\mathrm{PE}}, \quad (1)$$

with q the electron charge. $V_{\mathrm{gun\,offset}}$ and V_{analyzer} are power supplies of the order of -1 kV and -100 V, respectively. 1 kV power supplies with a stability and ripple of 0.1 eV are easily commercially available. The main power supplies V_{main}^+ and V_{main}^- are ± 25 kV and here a stability over the period of a few days and ripple of the order of 0.2 eV is less easily accomplished. Fortunately for the determination of the binding energy it is, according to Eq. (1), only necessary that $V_{\mathrm{main}}^- = -V_{\mathrm{main}}^+$. Thus drift and ripple may occur, as long as they do not affect this equality.

Long term drift compensation of the power supplies can then be accomplished by measuring the midpoint potential of a resistor divider chain that connects the outputs of both power supplies. The part of the ripple that affect $V_{\mathrm{main}}^+ + V_{\mathrm{main}}^-$ is measured by a capacitive divider. The drift and ripple compensation is accomplished by floating one of the two main power supplies on top of the small (magnitude <30 V) correction voltage. For the resistor chain we use two commercially available precision resistor dividers.[16] These dividers have a quoted temperature coefficient of 5 ppm/°C. As both dividers are in the same (temperature controlled) room and have the same power dissipation we expect part of their fluctuations to cancel so that after applying the feedback $V_{\mathrm{main}}^+ + V_{\mathrm{main}}^-$ is constant within 100 mV.

All electronics floating at ± 25 keV is battery powered as the use of (isolation) transformers tends to cause ac ripple. Using two 180 AmpereHours 6 V batteries for the filament power supply, the experiment can run uninterruptedly for up to six days.

The analyzers are designed to cover as much phase space as possible, while maintaining energy and momentum resolution. Instead of having a single aperture in each outgoing electron beam it has slits extending over $\pm 6.5°$ of azimuthal range. The analyzers are designed to measure simultaneously over this angular and hence momentum range. The polar angle θ of 44.3° is chosen so that the sum of the momenta of the detected electrons is equal to the momentum of the incoming electron if all three trajectories are in the same plane.

The analyzers simultaneously measure a range of energies and corresponding range in momenta. For the condition just mentioned it was assumed that the momenta of both detected electrons are equal. However, over the range of observed energies [at the largest pass energy used (500 eV) this energy window is 90 eV] the momentum p_1 and p_2 of the detected electrons can differ from the mean value by a small amount (up to 0.04 a.u. at 500 eV pass energy). The maximum error in the vectorial sum of both momenta is then 0.06 a.u., the mean error much smaller.

Using the geometry shown in Fig. 3, with the incident direction defining the z and x axis being in the mean horizontal scattering plane, the recoil momentum of the target is then directed approximately along the (vertical) y axis. Since $\theta_1 = \theta_2$ and $p_1 = p_2$ the magnitude of the recoil momentum is given by

$$p_y = p_1 \sin\theta(\sin\phi_1 - \sin\phi_2) \simeq p_1 \sin\theta(\phi_1 - \phi_2) \quad (2)$$

with ϕ_1 and ϕ_2 defined in Fig. 3. Because the angle defining slits lie on a cone with opening angle of 2θ there is also an

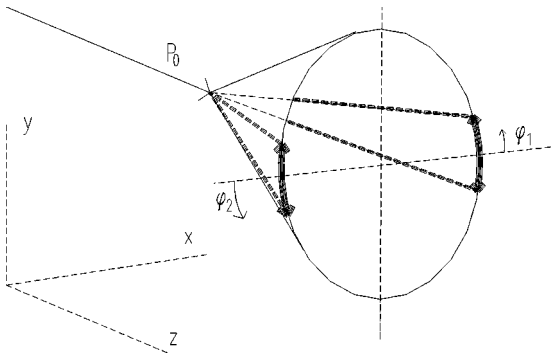

FIG. 3. Schematic view of the kinematics and the coordinate system used. The incoming electrons are directed along the z axis. The two electron analyzers accept those electrons that propagate along sections of a cone (cone half-angle 44.3°) as indicated. The angles ϕ_1 and ϕ_2 are measured experimentally. In the case of a coincident event, the difference of the incoming and outgoing momenta is directed approximately along the y axis.

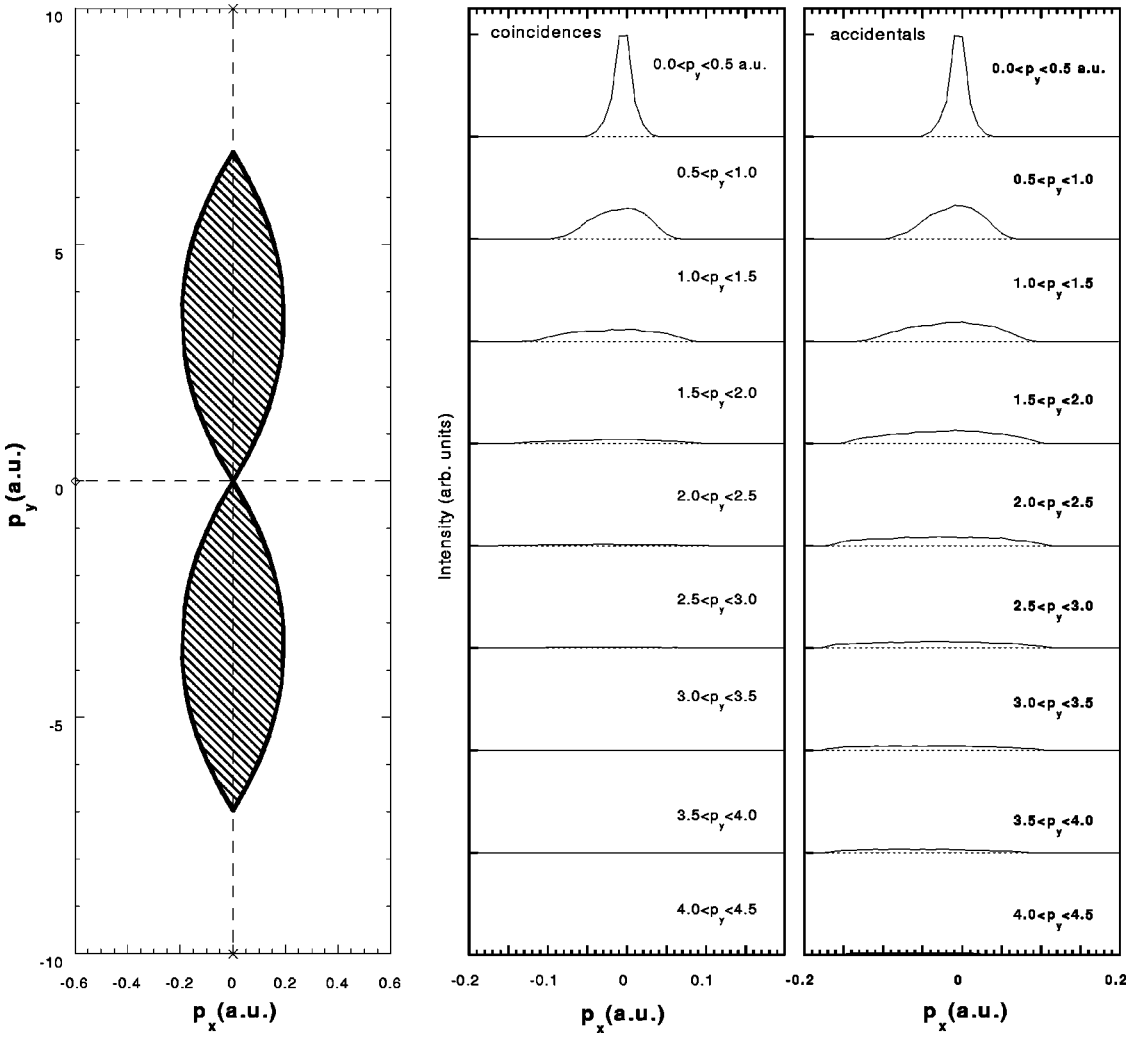

FIG. 4. (Left-hand panel side) accessible phase space of the spectrometer is drawn. In the central panel we plot the p_x component as a function of the measured p_y component for the case of graphite. For larger p_y values the intensity drops, as the momentum distribution of graphite is restricted to $\simeq |p| < 1.5$ a.u. (Right-hand panel side) distribution obtained from uncorrelated event. It is a measure of how efficient the spectrometer measures at those p_x, p_y combinations.

angle dependent x component of momentum of each detected electron. The p_x component, however, is much smaller and is given by

$$p_x = p_1 \sin\theta[\cos(\phi_1) - \cos(\phi_2)]. \quad (3)$$

The accessible momentum space is plotted in Fig. 4. Usually we neglect the spread in p_x as it is $<\simeq 0.1$ a.u. for momentum ranges $|p_y| < 1$ a.u., the typical range of valence band momentum densities. If a larger accuracy is required one can reject (by software) those events with a large value of $|p_x|$ (as it is measured) but this will somewhat limit the overall count rate. Compared to the asymmetric geometry the range of the p_x values is considerably smaller in the present spectrometer, for a given range of measured momenta.[10]

V. ELECTRON ANALYZERS

The scattered and ejected electron leaving the target specimen first find themselves within the high-voltage hemisphere, i.e., in a field free region. At the exit of the high-voltage hemisphere there is a 0.5 mm wide slit. It extends over an azimuthal range of $\pm 6.5°$. This is used for angular selection in low resolution measurements. For high resolution measurements one can further restrict the transmitted beam by turning in place 0.2 mm slits located in the high voltage area to intercept part of the beam. On the same turntable there is a set of small circular apertures, positioned along the cone. These are at known azimuthal angles and are used to calibrate the angular scale of the detector. Thus, changing the slit width and calibrating the angular scale can be accomplished without breaking the vacuum. The analyzer and optics are identical for both detected electrons.

After passing through the slits the electrons enter a decelerating lens system followed by a hemispherical analyzer. Conceptually these analysers and lens systems are very similar to the high-energy analyzer in the Flinders EMS spectrometer.[10] Between the high-voltage sphere (+25 keV) and the first lens element (+3 keV) the main deceleration of the electrons occurs. Thus the high-voltage sphere and the vacuum chamber wall and the first lens element are part of the electron optics. Care was taken that all these parts have the right spherical shapes, and carefully positioned to be concentric. The stack of lenses are slightly deformed slit lenses,

i.e., with the opening along the 44.3° cone. No focusing should occur along the azimuthal direction, i.e., the angular information is conserved. The slit lenses focus the incoming beam along the polar direction, and in this dimension an image of the target is formed at the entrance of a hemispherical analyzer (the window is formed by the target beam spot, 0.1 mm in size, the pupil is formed by the 0.2 or 0.5 mm slits).

Ideally the image of the slit at the entrance of the hemispherical detector would match the symmetry of the analyzer, i.e., all electrons would enter the analyzer at an equal distance to its center. Unfortunately, in that case both analyzers interfere with each other at the exit plane. Therefore, we had to rotate the hemispherical analyzer by 180°. All electrons enter the analyzer perpendicular, depending on the azimuthal angle at slightly different radial distances. The analyzer will still produce an image of the entrance slit at the detection plane, as all Keppler orbits are focused over 180°. However, the asymmetry of the elliptic orbit will change for a given electron energy, as a function of the entrance point. Thus for a given electron energy a deformed image will be formed in the detector plane. Changing the electron energy will change the deformed image.

Thus the electrons enter the analyzer (almost) perpendicular, but at a distance varying from R_0 to $R_0+\delta$. Inside the analyzer the electric field mimics a potential $V=c/r$. Here we choose the zero of the potential at ∞. In a $1/r$ potential electrons will move along a circular orbit if $E_{\mathrm{kin}}=-0.5E_{\mathrm{pot}}$. Thus at R_0 the analyzer has a pass energy $E_0=\mathrm{eV}_0$ if $c=2V_0R_0$. The potential of the base plate is thus $2V_0$.

Electrons entering at distance R_0 with energy E will be detected at a position (neglecting aberrations and fringe field effects):[17]

$$R_f=R_0\left(\frac{E}{2E_0-E}\right). \tag{4}$$

Consider for simplicity electrons with again a kinetic energy E_0 before entering the hemisphere at a radius $R_0+\delta$. Electrons entering at $R_0+\delta$ we will first see a decelerating field as the (constant) base plate potential does not match the $1/r$ potential at this position. The potential at $V(R_0+\delta)\simeq V(R_0)(1-\delta/R_0)$. Thus just inside the hemisphere the (kinetic) energy of the electron is reduced by $-V(R_0)\,\delta/R_0=2E_0\delta/R_0$. At $R_0+\delta$ electrons with a kinetic energy of $E'=E_0(1-\delta/R_0)$ will have a circular orbit. Thus the kinetic energy of the electron that had an energy E_0 before entering the hemisphere will be less than E' by $E_0\delta/R_0\simeq E'\delta/R_0$. It will thus be detected at

$$\begin{aligned}R_f&=(R_0+\delta)\left(\frac{E'(1-\delta/R_0)}{E'(1+\delta/R_0)}\right)\\&\simeq(R_0+\delta)\left(1-\frac{2\delta}{R_0}\right)\simeq R_0-\delta.\end{aligned} \tag{5}$$

The rather surprising result is that if an electron with energy E_0 enters the hemisphere at $R_0+\delta$ it will be detected closer to the center of the hemisphere at $R_0-\delta$.

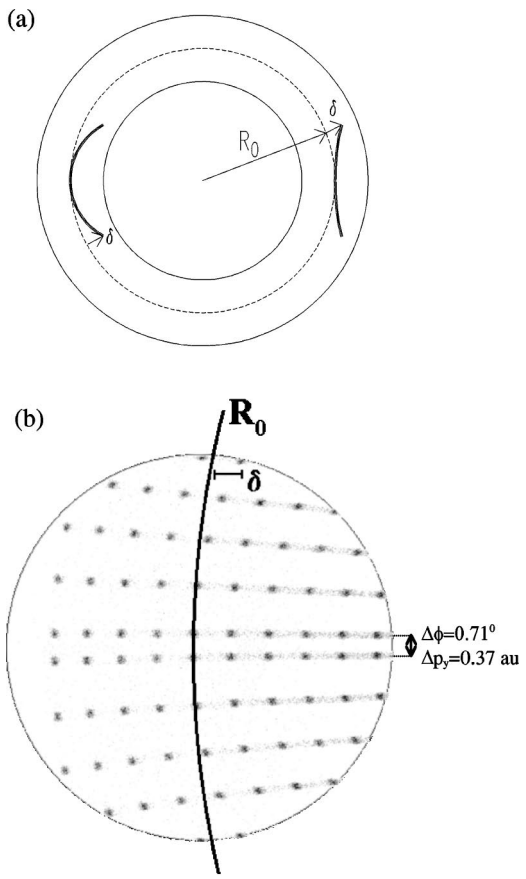

FIG. 5. (a) Schematic overview of the hemispherical electron analyzer, the central radius R_0, and the shape of the entrance aperture (distance varying from R_0 and $R_0+\delta$ from the analyzer center) and the corresponding image (distance varying from R_0 and $R_0-\delta$ from center); (b) Result of a calibration run. A series of peaks is shown for ten different incoming energies. The left–right dimension corresponds roughly to different energies, the up–down dimension to different angles. Also shown is the central radius, R_0 and the calculated deviation δ.

In the above we have neglected fringe fields. We have also neglected the fact that electrons entering the hemisphere at a distance $\neq R_0$ see a small retarding field and are thus perturbed by a weak lens. In the actual spectrometer $R_0=100\,\mathrm{mm}$ and the maximum value of δ is 2.7 mm. The change in kinetic energy at the hemisphere is thus $<5\%$, and the above approximations seem reasonable for this type of mismatch. This is corroborated by the experimental results.

The position sensitive electron detector itself is comprised of a pair of chevron-mounted channel plates and a resistive anode encoder. This part is equivalent to the one described by Storer *et al.*[10] Briefly, the fast timing signal is taken from the back of the second microchannel plate and decoupled using a transformer. It is used to start/stop the time to amplitude convertor (TAC). The signal from each corner of the resistive anode is amplified by a preamplifier followed by a main amplifier. The position of impact of the electron is calculated from the ratio of the amplitude of the four corner pulses to their summed amplitude.

The working and calibration procedure of the analyzer is illustrated in Fig. 5 using an elastic scattering experiment. The high-voltage sphere, lenses, and analyzers are at the

same potential as during the $(e,2e)$ measurement. The gun is tuned to a much smaller energy, in such a way that the elastically scattered electrons are detected. The calibration apertures are positioned in front of the 0.5 mm slit. Using a series of different gun energies we get intensities at the detector at a series of known energy-angle points. From Fig. 5 it is clear that for a certain energy the elastic peaks are located quite accurately on a segment of a circle. Circles corresponding to different energies are not concentric. This is due to the symmetry mismatch described above. In practice this is not a problem. The polynomial interpolation scheme developed by Caprari has no difficulty fitting the measured peak position and establishing the relationship between detector position and electron angle/energy combination.[18] No noticeable dependence of the energy and/or angular resolution was found on the angular position of the incoming electron. However, the lens settings corresponding to optimum focus differ slightly for the electrons at the lower and upper end of detected energy range. By changing the analyzer offset voltage we can move the elastic peak over the whole detector. If we measure an energy loss spectrum using 250 eV pass energy we get an energy resolution of about 0.8 eV using the whole of the detector, slightly better if we restrict the measurement to events from the central part of the detector (0.7 eV).

During an $(e,2e)$ experiment electrons over a wide range of energy impinge on the analyzer. From the output signals of the resistive anode in combination with the calibration constants we determine the energy and angle of each electron detected. The energy range that can be measured simultaneously in an analyzer is close to 20% of the pass energy.

The experiment is computerized and all nine signals (the TAC signal, corresponding to the time difference in detection of both electrons, and the amplitude of the signals of the four corners of both resistive anodes) are digitized simultaneously by a commercial ADC on a PC card (WIN30-DS from United Electronic Industries). The A/D conversion is triggered by the ''valid conversion'' output pulse of the TAC. These nine values are all stored to file, together with the current value of V_{analyzer}. The appropriate energy and momentum of each detected electron is calculated and from this we deduce the binding energy and momentum of the ejected electron. This information is stored in a two-dimensional array, both for the coincident and accidental background events. These calculations and the display of the results are done online. However, it is possible to reanalyze a measurement completely, using different input parameters (minimum signal heights, accepted angular and energy ranges, timing window for coincidences, etc.) using the complete information stored in the event-by-event file.

VI. DEFLECTORS

Operating the spectrometer as described above allows us to measure the energy-resolved momentum density of electrons with the momentum directed essentially along the y axis. If we have anisotropic samples (e.g., single crystals) it is important to be able to measure the energy-resolved momentum density for different slices through momentum space, i.e., not only along a vertical line through Γ of the first Brillouin zone. For this purpose we have a set of double deflectors along each outgoing trajectory. This allows us to direct electrons into the analyzers that leave the specimen with a polar angle that deviates by up to $\pm 1°$ from 44.3°. This is illustrated in Fig. 6. If we apply symmetrical voltages to each of the two detector sets so that both detectors measure electrons that were scattered over the same polar angle of say $44.3+\alpha$ we measure the energy resolved momentum density of electrons with a constant momentum component along the z direction. If we apply voltages antisymmetric to each set so that one detector measures electrons scattered over $44.3°+\alpha$ and the other $44.3°-\alpha$, we measure electrons with a constant momentum component in the x direction. In general we can shift the line along which we measure the y component of momentum by up to 1 a.u. away from zero momentum in any direction in the xz plane. The deflector plates are also required if we want to measure the density using incoming electrons with an energy different from 50 keV. Then the Bethe ridge angle of 44.3° will change slightly and we have to apply correction voltages to the plates, if we want to measure along a line through zero momentum.

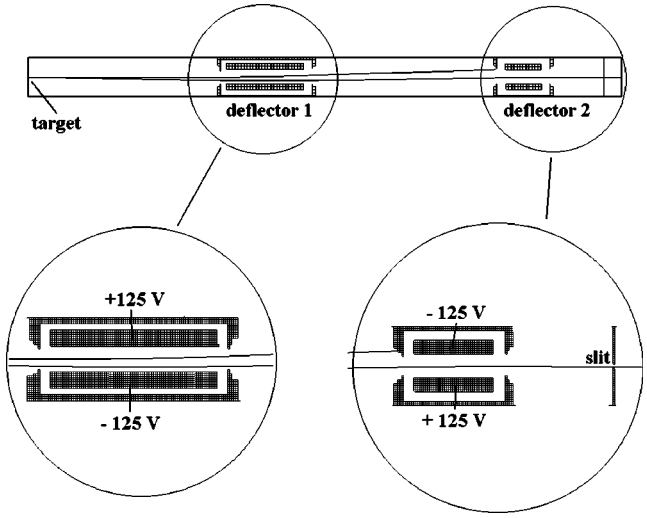

FIG. 6. Double deflectors used for measuring energy-resolved momentum densities away from the p_y axis. Deflector 2 is twice as far from the target as deflector 1. However, deflector 2 has only half the length of deflector 1 (but equal plate separation). Two rays are shown, one initially directed along the axis of the deflector system and one initially directed 1° away from the deflectors. By applying 125 V to the deflectors as indicated, the second beam leaves the deflector system traveling along its axis, whereas the first ray is intercepted.

The deflectors are computer controlled (via fiber optics) and several sets of spectra can be obtained simultaneously by cycling through different deflector settings. This allows us to measure momentum densities with $p_z \neq 0$ under exactly the same conditions (and hence relatively normalized) as the momentum density with $p_z = 0$.

VII. RESULTS

A 100 Å carbon film was used for testing the spectrometer. The first step is to establish coincidences between elec-

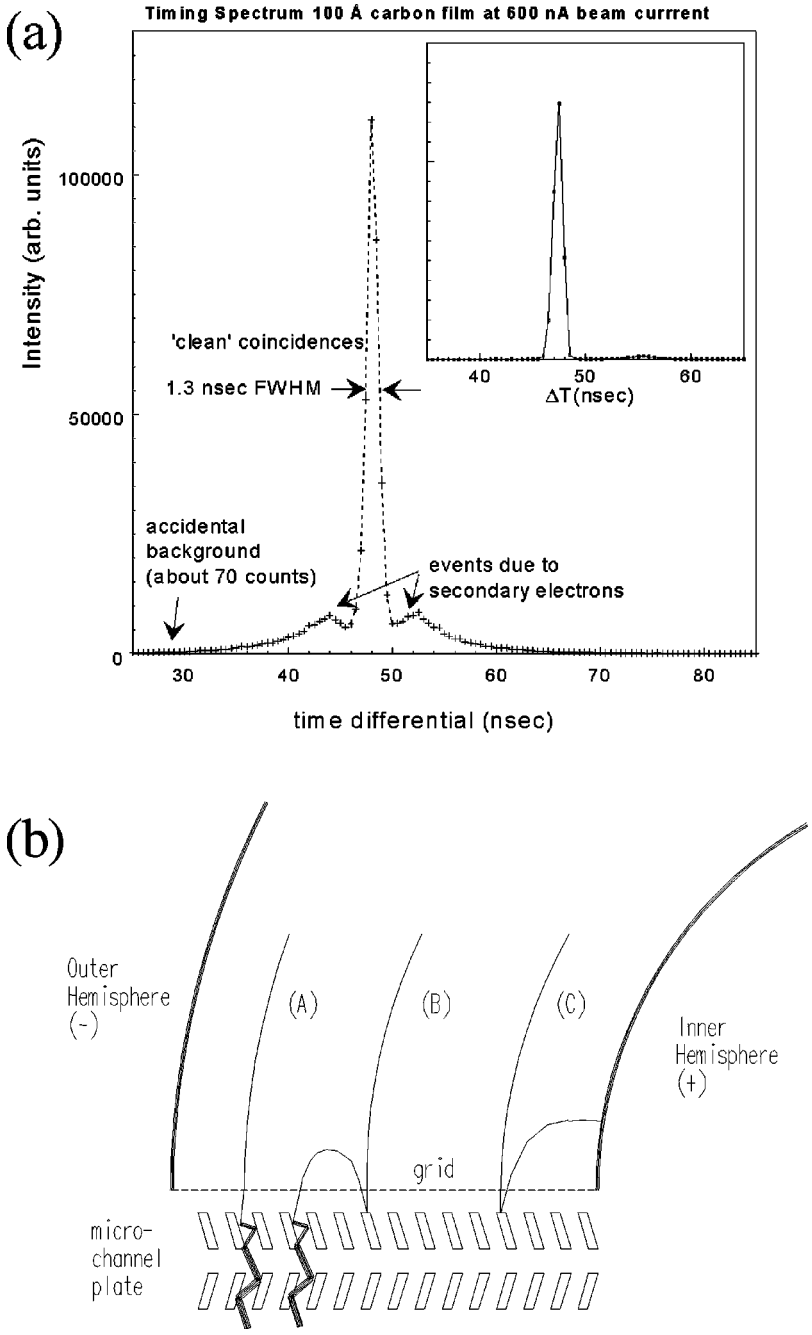

FIG. 7. (a) Timing spectrum of a 100 Å thick amorphous carbon film. There is a sharp main peak, with a minute background due to accidental coincidences. However, there are two broad peaks neighboring the main coincidence peak. The interpretation of these satellites is given in (b). The main line is due to electrons that are detected properly (trajectory A) in both start and stop detector. Some electrons hit the microchannel plate in the nonactive area, produce one or more secondaries that impinge on the plate later at a different position [trajectory (B)]. Near the inner hemisphere these secondary electrons are trapped by its attractive potential and the satellites are absent (trajectory C). Inset (a) shows the timing spectrum after a small (−80 V) bias was applied to the front of the first channel plate relative to the analyzer base plate.

trons in both detectors. Initially the timing spectrum was as shown in Fig. 7(a). After correcting for the flight time of the electrons in the analyzer we have a narrow coincidence peak of about 1.5 ns full width at half maximum. The signal to background ratio is about 1000:1 for 1 μA incident current, and a coincidence count rate of 60 counts a minute was obtained using the 0.2 mm slits and a pass energy of 250 eV. Using the 0.5 mm slits the coincidence count rate increases sixfold. Figure 7(a) shows, besides the timing peak proper, two satellite structures with an overall intensity comparable to that of the timing peak itself. These structures are only completely resolved using the narrow slits, and for the 0.5 mm slits become shoulders of the main peak. Analysis of both the main timing peak and the satellite counts showed that only the data obtained from the main peak showed sharp features in their energy-momentum distribution. Therefore, the satellite structures were discarded.

Further information about the nature of this satellite was obtained from the observation that it was not present for electrons impinging on the channel plates near the inner hemisphere. The interpretation of these observations are given in Fig. 7(b). Some electrons impinge on the nonactive part of the microchannel plate and create a secondary electron. If the secondary electron is generated near the outer hemisphere it will be pushed back onto the microchannel plate and could be detected there, at a time and place considerably different from the original position of impact. If this process occurs for the detector that starts the TAC, then the measured time difference between start and stop will be too short. If this process occurs in the stop channel, the observed time difference is too long.

If the secondary electron is generated near the inner hemisphere it can be attracted to this hemisphere by its positive potential with respect to the exit grid and channel plate

front, both being at the central (base plate) potential. This problem was solved by applying a negative bias to the front of the first channel plate relative to the grid at the exit of the analyzer. The satellites disappeared.

A complication of using these multiple-parameter detectors is the response function. Many different combinations of energy E_1, E_2 will result in the same binding energy ε, and many different combinations of ϕ_1, ϕ_2 result in the same p_y. Unfortunately, not each combination of ε, p_y is measured with the same efficiency. Near the extremes of the range of either ϵ or p_y there are only very few combinations that contribute. On top of this the detection efficiency of the channel plates varies across the sensitive areas. Thus, the spectral momentum density has to be obtained by dividing the observed count rate $N(\epsilon, p_y)$ by the spectrometer response function $R(\epsilon, p_y)$. This can be obtained from uncorrelated events. The singles count rate does not contain information about the electronic structure of the target. Thus the position sensitivity for singles counts is determined by the individual detector response function $F_1(E_1, p_{y1})$ and $F_2(E_2, p_{y2})$, i.e., as a function of energy and the p_y component of the detected electrons. The response function of the coincident experiment is obtained by taking a number of uncorrelated singles events from both detectors, and calculating the fictive binding energy ε and momentum p_y that would apply to the target electrons if both electrons originated from the same collision event. The distribution of these fictive coincidences is determined by the detector response functions only and thus provide an experimental estimate of the spectrometer response function.

Traditionally this response function is obtained by analyzing those events that are *not* coincident with the timing peak in the TAC spectrum.[19] Although the very low accidental coincidence rate is in itself beneficial, it has as a negative side effect that we cannot use them as a convenient way to determine the response function of the spectrometer, as in our case not enough statistics is accumulated. Therefore we used an alternative method. Singles measurements for each detector were performed sequentially with the same microchannel plate voltage, signal thresholds and accepted angular and energy range of the detectors. The experimental coincidence response function $R(\epsilon, p_y)$ was then obtained from the frequency distribution of ε, p_y as calculated for all possible combinations of pairs of singles events given by the singles response functions $F_x(E_x, p_{yx})$:

$$R(\epsilon, p_y) = \int\int F_1(E_1, p_{y1}) \times F_2(E_0 - E_1 - \varepsilon, p_y - p_{y1})\, dE_1\, dp_{y1}. \quad (6)$$

Here we use energy and momentum conservation to establish the relation between E_1, E_2, and ε and p_1, p_2, and p_y. This procedure establishes a very smooth response function in minutes.

The energy resolution of the spectrometer was established by measuring the C $1s$ core level of a highly oriented pyrolytic graphite (HOPG) sample. A resolution full width at half maximum (FWHM) of 1.8 eV was found, using 250 eV pass energy. This is very similar to the resolution obtained at Flinders *without* an energy monochromator for the incoming electrons.[20] In that case significant improvements were found using a monochromator, indicating that space-charge induced energy broadening in the electron gun is a major contribution to the energy resolution. Similar improvements are planned for the current spectrometer.

In order to test the alignment and the working of the deflection plates we measured a HOPG film, prepared as previously described.[21] Originally we measured electrons without a momentum component in the z direction, coinciding with the c axis of the HOPG. By applying voltages to the deflectors we effectively changed the detector angles and tuned in to electrons with a constant p_z momentum component of 0.7 a.u. The results are shown in Fig. 8 which shows the measured intensity as a function of p_y at the binding energy intervals as indicated. In the case of $p_z = 0$ we only see one dispersing structure (the σ band), the π band having a node (hence zero density) in the $p_z = 0$ plane. In the case of $p_z = 0.7$ a.u. we see two structures, the σ as well as the π band. The deflectors turn out to be an effective way to access different parts of momentum space.

The reduced influence of elastic scattering can be seen in the small ratio of the intensity near zero momentum relative to the intensity at the band position away from the bottom of the band. At a binding energy $\varepsilon = 10$ eV the background near $p_y = 0$, $p_z = 0$ is now up to 10 times smaller than the band intensity, whereas using the Flinders spectrometer the background was at most 3 times smaller than the peak intensity.

The shape of these energy-resolved momentum distributions of a solid are much narrower than those of atomic and molecular orbitals, and are hence a more critical test of the spectrometer's momentum resolution. The FWHM of the narrowest peak observed is about 0.25 a.u. From Fig. 8 it is clear that the peaks of the momentum distribution disperses strongly with energy. Thus the observed width is not only determined from the momentum resolution, but also by the width of 2 eV (in combination with the finite energy resolution) over which the intensity was integrated in order to determine these momentum profiles. The observed momentum densities are thus not inconsistent with the expected momentum resolution of around 0.1 a.u.

The effects of inelastic multiple scattering are most readily seen in the energy spectra. In Fig. 9 we show the spectrum at zero momentum of a HOPG film (estimated thickness 200 Å) and a 50 Å thick, annealed, amorphous carbon film. The intensity drops off rather quickly at binding energies exceeding that of the bottom of the σ band for the amorphous carbon film, whereas the thicker HOPG film shows a second peak due to extrinsic plasmon energy losses. However at binding energies around 10 eV the HOPG intensity is less than the amorphous carbon one, as the suppression of π intensity is less complete in the latter, due to limited long range order. As an inset we show at the same energy-scale the carbon (HOPG) $1s$ core level. The width of this level is 1.8 eV, and is an upper estimate of the spectrometer energy resolution (inhomogeneities in the sample may contribute to the observed width as well). The width of the valence band spectrum is much larger than that of the core level.

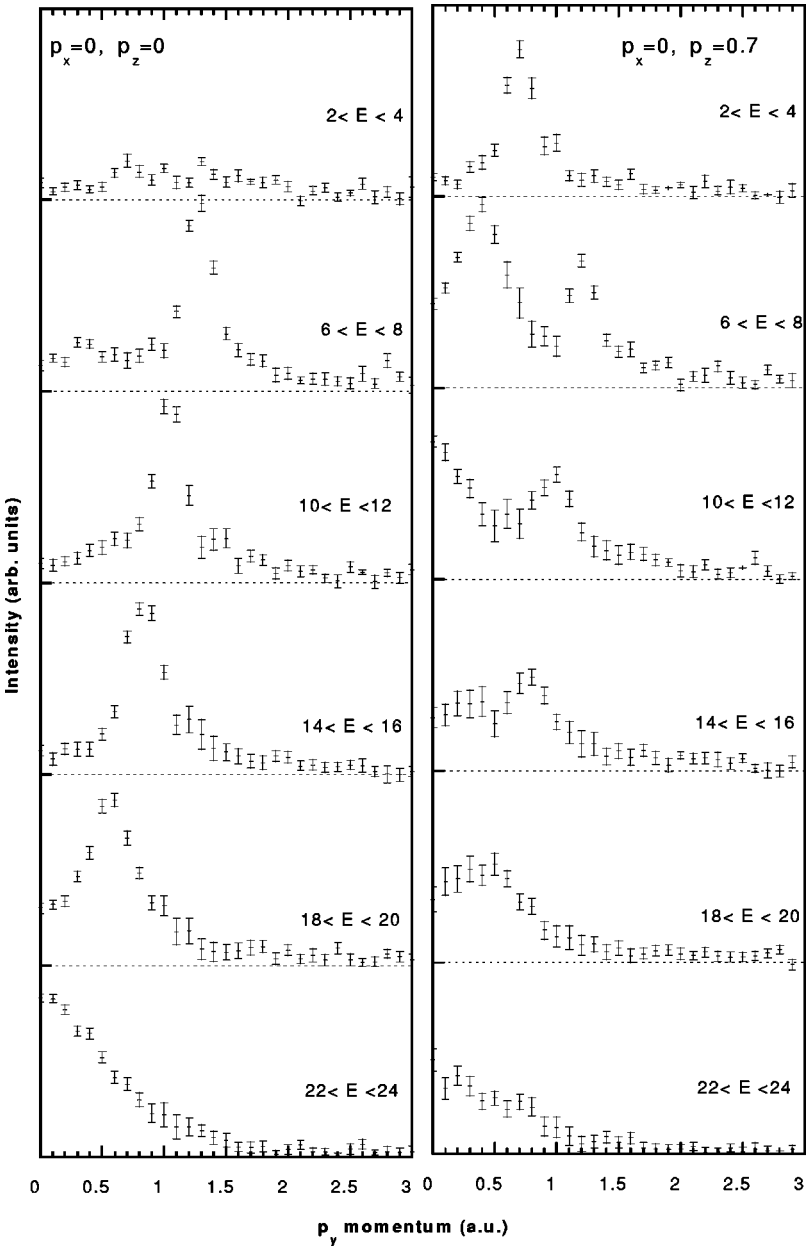

FIG. 8. Momentum densities at selected binding energy ranges for highly oriented pyrolytic graphite. The *c* axis of HOPG is approximately along the *z* direction. Without deflector voltages we measure densities $p_z \simeq 0$ and we only observe the σ band (left-hand side panel). By applying voltages to the deflector we can measure for $p_z \simeq 0.7$ a.u. and the spectra are dominated by the π band. Note the large intensity difference between the maxima and minima, indicating that elastic scattering effects along the incoming and outgoing trajectories are small.

Part of the intensity at binding energies exceeding 20 eV is due to intrinsic satellites, a consequence of electron–electron correlations, and would be observed as well if the film was so thin that multiple scattering would not occur. An estimate of the expected shape near Γ, i.e., zero momentum (for an infinitely thin film) is shown by the solid line which is obtained from the spectral function derived from a many-body calculation.[22] No attempt was made to add energy and or momentum resolution to this theory, the experimental energy resolution being small compared to the observed lifetime broadening of the spectral function. Even so, the measured intensity resembles the calculated peak shape quite nicely. It therefore seems that we have succeeded in obtaining direct spectroscopic evidence on the shape of the spectral function of this form of carbon.

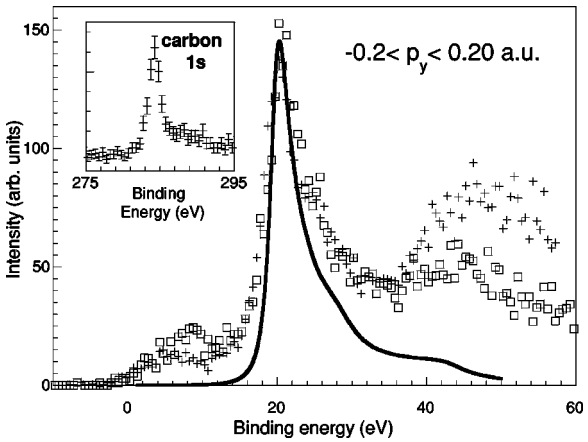

FIG. 9. Energy plot for HOPG (+) film and a 50 Å thick annealed evaporated carbon film (□) for events with momentum $|p| < 0.2$ a.u. The peak near 20 eV corresponds to the bottom of the σ band and is much broader then the energy resolution, as is clear from the core level spectrum of HOPG (see inset). The solid line is the result of a many-body calculation and follows the experimental spectrum surprisingly well.

VIII. DISCUSSION

In a recent review Dennison and Ritter proposed as their ''ideal EMS spectrometer'' a spectrometer using similar ki-

nematics as the above but working at twice the energy.[23] Extrapolating from our experience this configuration would work reasonable well with just a single pair of detectors rather than the 60 pairs proposed in their article. The main challenge would be the stability of the high voltage and the design of the 50 keV retarding electrostatic lens system. As the gain in higher energies is only to reduce multiple scattering, the same effective result could be obtained by decreasing the electron beam spot size and simultaneously improving the control and stability of the sample positioning. This would allow the user to choose more effectively the thinnest spot of the sample (with as a tradeoff the higher current density, that may introduce damage to the sample). Thus reducing the beam spot from 0.2 to 0.1 mm (diameter) (without introducing a large angular spread) and positioning the sample with a precision and a stability of 0.1 mm could approximately half the effective thickness of the sample, resulting in an improvement of the same order as doubling the energy.

With this spectrometer, we hope to show that EMS can contribute to the understanding of the electronic structure. Since in EMS real momenta are measured, the technique is equally applicable to amorphous and disordered materials as well as single crystals. Until now, studying the electronic structure of the valence band of a solid has been almost synonymous with measuring the dispersion. A unique relation between a binding energy and the (crystal-)momentum exists only if one makes the simplifying assumption that the only effect of electron–electron interaction is that it modifies the periodic potential that the electron probes. This is quite an oversimplification, as the shapes of spectral functions of even simple free-electron materials show.[4] Due to the simplicity of the plane-wave impulse approximation, well justified at these high energies, one can focus directly on the electronic structure, and the effects of electron–electron correlations. Although in the case of crystals photoemission techniques provide information on the dispersion of bands that have, especially near the Fermi level, an energy resolution that presently exceeds that of EMS by orders of magnitude, quantitative analysis of peak shapes and intensity is problematic. Therefore, we think that EMS, in spite of its present limited energy resolution, can contribute significantly in enhancing the understanding of the electronic structure beyond the mean field level.

ACKNOWLEDGMENTS

This spectrometer could not have been built without the skilled support provided by the technical services of the Research School of Physical Sciences and Engineering. M. V. is supported by a fellowship of the Australian Research Council.

[1] I. McCarthy and E. Weigold, Rep. Prog. Phys. **54**, 789 (1991).
[2] V. Neudatchin, Y. V. Popov, and Y. F. Smirnov, Phys. Usp. **42**, 1017 (1999).
[3] E. Weigold and I. McCarthy, *Electron Momentum Spectroscopy* (Kluwer Academic/Plenum, New York, 1999).
[4] L. Hedin, J. Phys.: Condens. Matter **11**, R489 (1999).
[5] M. Vos and M. Bottema, Phys. Rev. B **54**, 5946 (1996).
[6] R. Camilloni, A. G. Guidoni, R. Tiribelli, and G. Stefani, Phys. Rev. Lett. **29**, 618 (1972).
[7] A. Ritter, J. Dennison, and J. Dunn, Rev. Sci. Instrum. **55**, 1280 (1984).
[8] P. Hayes, M. Bennet, J. Flexman, and J. Williams, Rev. Sci. Instrum. **59**, 2445 (1988).
[9] J. Lower, S. Bharathi, Y. Chen, K. Nygaard, and E. Weigold, Surf. Sci. **251–252**, 213 (1991).
[10] P. Storer, R. Caprari, S. Clark, M. Vos, and E. Weigold, Rev. Sci. Instrum. **65**, 2214 (1994).
[11] M. Vos, E. W. A. S. Kheifets, S. Canney, B. Holm, F. Aryasetiawan, K. Karlsson, and E. Weigold, J. Phys.: Condens. Matter **11**, 3645 (1999).
[12] J. Kirschner, O. Artamonov, and S. Samarin, Phys. Rev. Lett. **75**, 2424 (1995).
[13] S. Rioual, S. Iacobucci, D. Neri, A. Kheifets, and G. Stefani, Phys. Rev. B **57**, 2545 (1998).
[14] W. Nakel, Phys. Rep. **243**, 317 (1994).
[15] H. Schmoranzer, H. Wellenstein, and R. Bonham, Rev. Sci. Instrum. **46**, 285 (1975).
[16] Ross Engineering Inc., 45 keV matched pair 5 ppm voltage divider 90 MΩ each.
[17] C. Kuyatt and J. Simpson, Rev. Sci. Instrum. **38**, 103 (1967).
[18] R. Caprari, Comput. Phys. **7**, 336 (1993).
[19] M. Vos, R. Caprari, P. Storer, I. McCarthy, and E. Weigold, Can. J. Phys. **74**, 829 (1996).
[20] S. Canney, M. Brunger, I. McCarthy, P. Storer, S. Utteridge, M. Vos, and E. Weigold, J. Electron Spectrosc. Relat. Phenom. **83**, 65 (1997).
[21] M. Vos, P. Storer, S. Canney, A. Kheifets, I. McCarthy, and E. Weigold, Phys. Rev. B **50**, 5635 (1994).
[22] A. Kheifets (unpublished).
[23] J. Dennison and A. Ritter, J. Electron Spectrosc. Relat. Phenom. **77**, 99 (1996).